Assessment of Urban Heat Islands in an Eastern Amazonian city

Lucas Lima Raiol[1], Yuri Antonio da Silva Rocha [1], Dayla Carolina Rodrigues Santos [2], Aline Maria Meiguins de Lima [1], Andrés Velastegui-Montoya [3, 4]

[1] Institute of Geosciences, Federal University of Pará (UFPA), Brazil- lucas.raiol@ig.ufpa.br, eng.yurirocha@gmail.com, ameiguins@ufpa.br
[2] Amazon Institute of Family Agriculture, Federal University of Pará (UFPA), Brazil – dayla.santos@ineaf.ufpa.br
[3] Centro de Investigación y Proyectos Aplicados a las Ciencias de la Tierra (CIPAT), ESPOL Polytechnic University, Ecuador
[4] Faculty of Engineering in Earth Sciences FICT, ESPOL Polytechnic University, Ecuador – dvelaste@espol.edu.ec

Keywords: Land Surface Temperature, Urban Heat Island, Amazon, Google Earth Engine, Moran Index.

Abstract

The increase in heat islands in large cities, especially in tropical areas, has been a significant problem, as the rise in temperature can cause health issues for people. Therefore, this research aimed to analyze changes in land surface temperature (LST) and urban heat islands (UHI) in 1986 and 2023. The methodological procedures were carried out in four steps: I) Calculation of LST and UHI using the Landsat collection; II) Zonal statistics of the mean, the median, the minimum, maximum, and standard deviation of LST and UHI in each neighbourhood; III) Kruskal-Wallis Test applied to the average LST between 1986 and 2023; and IV) Assessment of the spatial autocorrelation of neighbourhoods using Bivariate Global and Local Moran’s I Index between LST and UHI. The results showed that in 2023, there was an increase in heat islands in central city neighbourhoods compared to 1986, as demonstrated by the Kruskal-Wallis test, which showed significant differences in LST. The global Moran’s I Index presented a value of 0.642, indicating a robust spatial autocorrelation in local studies. The neighbourhoods that showed high correlations were Campina, Cidade Velha, Cremação, Condor, Fátima, Jurunas, Nazaré, Pedreira, Reduto, São Braz, and Umarizal. The neighbourhoods that showed low correlations were Águas Lindas, Aurá, Curió-Utinga, Guanabara, and Parque Guajará. These results are directly linked to the intensification of urbanization and low vegetation cover, especially in central areas of the city, which showed a high correlation. These findings can aid decision-makers and support urban planning, focusing on neighbourhoods with higher average temperatures.

1. Introduction

Global warming induced by climate change is an alarming phenomenon intensely affecting the 21st century (Kafy et al., 2022). Therefore, it causes long-term temperature variations, yearly precipitation, sea level increases, and the frequency of hydrometeorological dangers that threaten most of the world’s population (Rahaman et al., 2022). One of these consequences is the Urban Heat Islands (UHI), a significant concern due to urbanization and industrialization. The excessive heat generated by urban structures and anthropogenic heat sources contributes to increased temperatures in urban areas, creating UHI Intensity (Rizwan et al., 2008). This issue is particularly pronounced in cities with large populations and extensive economic activities (Zhou et al., 2015).

UHI research has become popular in recent decades due to the impacts of heat stress on the population and the environment, mainly affecting children and the elderly due to respiratory difficulties, heat stroke, heat exhaustion, cramps, and mortality (Diem et al., 2024). Climate change acts as a catalytic agent for UHI, exerting its intensification, with its main causes at the local, microclimate, and mesoscale being the ability of building materials to store heat, heat production, the alteration and minimization of wind speed as a function of surface roughness, and the increased absorption of solar radiation by albedo surfaces (Almeida et al., 2021; Diem et al., 2024). Other consequences are the increased energy demand in the use of electronics for cooling and thermal comfort, which drives the increase in the use of electricity, in addition to the emission of greenhouse gases, reduced water availability, droughts, and changes in biodiversity (Diem et al., 2024).

In the Brazilian Amazon, the increase in LST is also associated with deforestation and fire foci in protected areas and indigenous lands (Silva et al., 2023). Several studies have found a significant increase in LST and UHI, with urban areas being the most affected compared to rural areas (Carrasco et al., 2020; Espinoza et al., 2023; Furtado et al., 2024). Among the applications of UHI and LST, the use of thermal sensors from the MODIS and Landsat satellites stands out, the latter being the most widespread in the world, as it is appropriate for long-term monitoring, while MODIS provides a daily to monthly analysis (Almeida et al., 2021; Diem et al., 2024).

The municipality of Belém in the Eastern Amazon is a great important metropolis. Given this, the city has been affected by Land Surface Temperature (LST) rising over the years, which causes thermal stress on the population (Silva et al., 2021). These trends were observed due to human pressure, vegetation suppression, and disorderly urban expansion in many cities worldwide (Waleed et al., 2023; Furtado et al., 2024). Accordingly, this study aimed to analyze the changes in the LST and UHI in the years 1986 and 2023 in the urban area of the Belém, using remote sensing techniques and a cloud computing-based platform to support decision-makers and urban planners.

2. Study Area

The municipality of Belém is the second most populous city in the northern region of Brazil, with 1,303,403 inhabitants and a territory of 1,059.466 km² (IBGE, 2022). Considering the island and continental portions, the municipality of Belém is divided into 8 (eight) administrative districts, encompassing 39 (thirty-nine) islands and 71 (seventy-one) neighbourhoods (IBGE, 2010; Moreira; Vitorino, 2017). The study area, which refers to the urban area (Figure 1), has 48 neighbourhoods and 177.26 km² (IBGE, 2010). According to the Köppen climate classification, the municipality of Belém is in two categories, with the southern side corresponding to the urban area in Af (no dry season) and the northern region in Am (monsoon) (Alvarez

et al., 2013). The municipality of Belém has an average annual rainfall of 3,000 to 4,000 mm and average temperatures of 26 ± 0.4ºC, with maximum and minimum temperatures ranging from 31.5 ± 0.7 to 22.0 ± 0.3ºC, respectively, with a dry period from July to November and rainy periods from January to April (Silva Junior et al., 2012; Alvarez et al., 2013; Furtado et al., 2024).

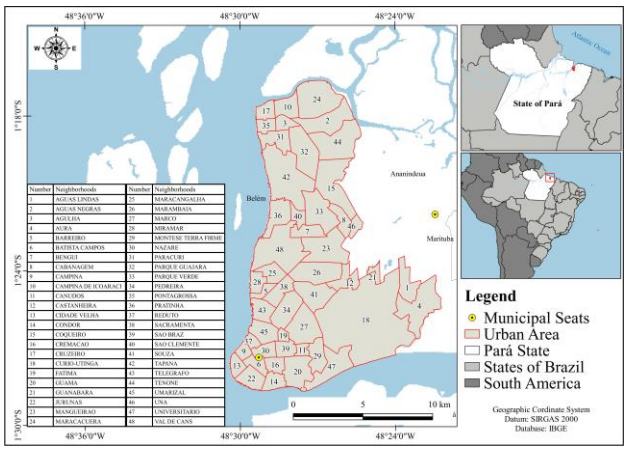

Figure 1. Study area.

3. Methodology

3.1 Data Gathering and Framework

The methodological procedures (Figure 2) involved two phases: I) data processing involving the acquisition and retrieval of the LST and calculation of the UHI using the cloud computing-based platform (Google Earth Engine - GEE) (Velasteguí-Montoya et al., 2023); and phase II) in which the data analysis was performed involving descriptive statistics and Moran Index calculation. All phases are described in the following sections. The codes used to retrieve LST and calculate UHI on GEE are available for Landsat 8 OLI/TIRS (https://code.earthengine.google.com/928179c88c4600963817ba7b52ccc513) and Landsat 5 TM (https://code.earthengine.google.com/3dd0b31f9b58a8fd44de1c3d219b4dd5).

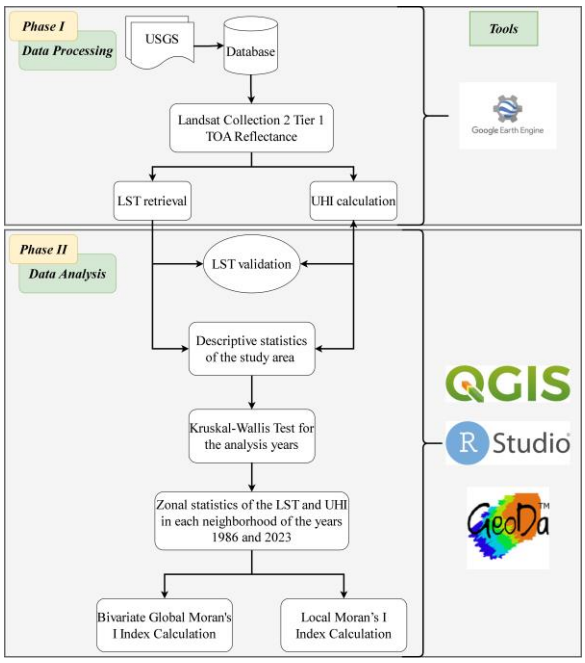

Figure 2. Methodology flowchart.

3.2 Land Surface Temperature Retrieval

Images from Landsat Collection 2 calibrated top-of-atmosphere (TOA) reflectance were used through GEE. The pre-processing images started with select images based on a cloud filter by 5%, corresponding to the dates 07/17/1986 (Landsat 5 TM) and 07/23/2023 (Landsat 8 OLI/TIRS). The choice of these dates is justified because July is part of the dry period with fewer clouds, as well as to avoid seasonal variations and bias. The resulting images for each year were cropped to the study area. The thermal bands of Landsat-5 TM and Landsat 8 OLI/TIRS were used to estimate the LST, bands 6 and 10, respectively. Band 11 of Landsat 8 OLI/TIRS is not used because it has less calibration than 10 (Waleed and Sajjad, 2022).

The procedures adopted to estimate the LST were based on Waleed and Sajjad (2022), in which the Thermal bands are used to convert Digital Numbers (DN) into spectral radiance (Lλ) using equations (1) and (2). The resulting top of atmospheric radiance (Lλ) is in watts/(m2 × ster × μm) shown in equation (1).

$$L_\lambda = \left(\frac{L_{MAX} - L_{MIN}}{QCAL_{MAX} - QCAL_{MIN}}\right) \times (QCAL - QCAL_{MIN}) + L_{MIN} \quad (1)$$

where *L*MAX = maximum spectral radiances (15.600 for TM), *L*MIN = minimum spectral radiances (1.238 for TM), QCALMAX = maximum Digital Number (DN) value (255), QCALMIN = minimum Digital Number (DN) value (1), QCAL = Digital Number value of band 6.

The values of LMAX, LMIN, QCALMAX, and QCALMIN are obtained from the metadata file attached to each Landsat image. The Landsat 8 OLI thermal band, the top of atmospheric radiance (*Lλ*), is calculated using the following equation (2).

$$L_\lambda = M_L \times QCAL + A_L \quad (2)$$

where *ML* = multiplicative rescaling factor for specific band (0.0003342), QCAL = digital numbers of band 10, and *AL* = additive rescaling factor for specific band (0.1).

The TOA brightness temperature was calculated from spectral radiance using the following equation (3):

$$T_B = \frac{K_2}{\ln\left(\frac{K_1}{L_2} + 1\right)} \quad (3)$$

where *TB* =at-satellite brightness temperature in Kelvin (K), *Lλ* =spectral radiance, *K1* and *K2* =calibrated constants depending on the sensor, and it can be found in the metadata files.

The emissivity correction depends on the category of land use, and it is evaluated using the Normalized Difference Vegetation Index (NDVI) per pixel value (Waleed and Sajjad, 2022). Equation (4) is used to evaluate emissivity corrected LST:

$$S_T = \frac{T_B}{1 + \left(\frac{\lambda \times T_B}{\rho}\right) \times \ln \varepsilon} - 273.15 \quad (4)$$

Where *ST* = land surface temperature in (°C), *TB* = at-satellite brightness temperature (K), λ = wavelength of emitted radiance (11.5 μm), ρ = 1.438 × 10−2 mK, ε = emissivity (ranges from 0.97 to 0.99).

Emissivity can be calculated by using equation (5), which is:

$$\varepsilon = 0.004Pv + 0.986 \quad (5)$$

Where *Pv* = proportion of vegetation.

The proportion of vegetation *Pv* can be calculated using the following equation (6);

$$Pv = \left(\frac{NDVI - NDVI_{\min}}{NDVI_{\max} - NDVI_{\min}} \right)^2 \quad (6)$$

In which *NDVI*, *NDVImin*, and *NDVImax* are per pixel value of NDVI, minimum NDVI, and maximum NDVI values, respectively.

3.3 Urban Heat Island Calculation

The UHI effect is a relative concept, and its degree indicates the temperature difference between the city centre and surrounding areas that show lower temperatures (Xu et al., 2013). The UHI is also associated with LULC and the geographic distribution of vegetation (Rahaman et al., 2022).

A normalized method is adopted to compare UHI due to observed variations in LST within a year (Faisal et al., 2021; Rahaman et al., 2022). UHI is given as Equation (7)

$$UHI = \frac{Ts - Tm}{SD} \quad (7)$$

Subsequently, the resulting UHI values were reclassified according to the classes and proportions of value ranges defined by Xu et al. (2013). Table 1 presents the UHI classes and their corresponding ranges.

Ranges	Classes
<0	Green Island
0-1	Weak UHI
1-2	Medium UHI
2-4	Strong UHI
>4	Extremely Strong UHI

Table 1. Classification of the Urban Heat Island (UHI) intensity levels.

3.4 Land Surface Temperature Validation

Data from the National Institute of Meteorology (INMET) with station codes 82191 and A201 were used to validate the LST. The INMET data were collected on the same dates as the images (July 17, 1986, and July 23, 2023) and, at times, approximating the Coordinated Universal Time (UTC) of the Landsat imagery, as described in Table 2. Subsequently, sampling of LST raster values was performed according to the coordinates of each station.

Weather Station code	82191	82191	A201
Date	17/07/1986	23/07/2023	23/07/2023
LST (ºC)	27.51	27.57	29.00
Weather station (ºC)	26.60	27.10	29.00
Weather station measurement time (UTC)	12:00	12:00	13:00
Landsat imagery measurement time (UTC)	12:46	13: 23	

Table 2. Information about LST and Air temperature values from Landsat and weather stations in the study area.

Afterwards, the Pearson correlation (ρ), the Coefficient of Determination (R^2), and the Root Mean Square Error (RMSE) were applied in the RStudio software as validation metrics. The Pearson correlation (ρ) assesses the strength and linear direction between the variables, where 1 indicates a perfect positive linear association, and -1 indicates a perfect negative linear association. R^2 is a statistical measure that indicates the proportion of the variance in the dependent variable that is predictable from the independent variable(s), where a value of 1 indicates that the model explains all the variation. The RMSE is a metric for evaluating forecast models, measuring the average of the squared errors. The lower the RMSE, the better the model fits the data.

3.5 Statistical Analysis

The statistical analysis was conducted using RStudio software, where the non-normality of the data (p-value < 0.05) was first verified using the Shapiro-Wilk test. Following this, the non-parametric Kruskal-Wallis test was performed to determine whether there were significant differences in the LST averages in the neighbourhoods between 1986 and 2023. The LST and UHI averages were extracted for the neighbourhoods in QGIS, using the zonal statistics tool to obtain the mean, median, maximum, minimum, and standard deviation to identify the behaviour patterns of these two variables.

3.6 Moran Index Calculation

The results of the LST and UHI averages for the neighbourhoods were used to analyze Moran’s I Index. The Bivariate Global and Local Moran’s I Index assessed the spatial autocorrelation between the neighbourhoods. The values used were the LST and UHI averages for 1986 and 2023. In general, the Moran’s I Index tests the null hypothesis of spatial independence; in this case, a value of zero indicates no spatial correlation, positive values (between 0 and +1) indicate direct correlation and negative values (between 0 and -1) indicate inverse correlation (Câmara et al., 2004). This analysis was conducted using Geoda software.

4. Results and Discussion

4.1 Land Surface Temperature Validation Analysis

The results obtained from the LST from Landsat showed a strong positive correlation (ρ = 0.99), with the coefficient of determination explaining 97% of the variation in the LST data in the linear model (R^2 = 0.97). The Root Mean Square Error (RMSE) calculated was 0.59. Therefore, the results are satisfactory despite the limited number of measurements from meteorological stations in the years analyzed. Another point that may influence future research to improve the accuracy of the Landsat LST is to relate it to values measured from automatic meteorological stations. According to Table 2, station A201 (an automatic station) presented the same value of 29.00 ºC as measured in the Landsat image from 2023, indicating that automatic stations may offer greater reliability in collecting measured values.

The accuracy of the LST generated from Landsat images obtained satisfactory results when compared to Sentinel 3 SLSTR images, which are optimized to measure LST with a systematic uncertainty of 1.3 K and a precision of 1.3 (Batoni et al., 2024). Other research on the LST generated from Landsat was also compared with in situ measurements, meteorological stations, and with MODIS LST retrievals, which presented

results with high accuracy (Wang et al., 2020; Aslan and Koc-San, 2023; Ghasempour et al., 2023; Batoni et al., 2024).

4.2 Land Surface Temperature Changes

Figure 3 shows the temperature variation in the urban area of Belém. It was possible to observe an expansion of higher temperatures in other neighbourhoods, primarily towards the north. In 1986, the urban area had an average temperature of 27.17 ºC ± 1.60 ºC, which increased to 28.67 ºC ± 1.80 ºC by 2023, representing a rise of 1.5 ºC over these 37 years (Table 3).

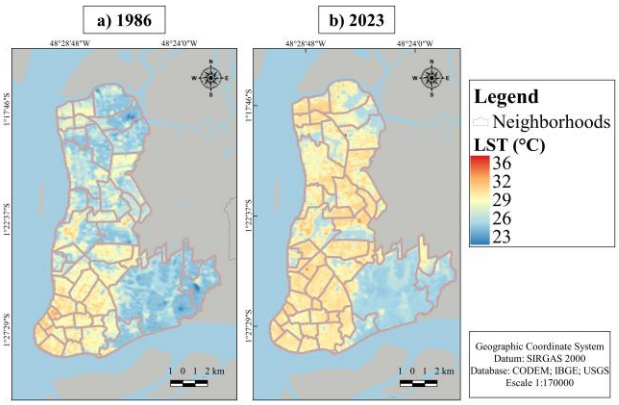

Figure 3. LST of the years 1986 and 2023 for the urban area of the Belém.

This increase of 1.5 ºC represents an average rise of 0.04 ºC per year over the 37 years. This increase in the LST average reflects the rise in thermal amplitude during these periods, where the minimum temperature increased from 22.80 ºC in 1986 to 25.17 ºC in 2023 (Table 3). Similarly, the maximum temperature rose from 32.43 ºC to 36.88 ºC in 2023.

LST values	1986	2023
Minimum Temperature (ºC)	22.80	25.17
Maximum Temperature (ºC)	32.43	36.88
Mean (ºC)	27.17	28.67
Standard Deviation (ºC)	1.60	1.80

Table 3. Descriptive statistics for study area in the years 1986 and 2023.

The increase in mean LST over the study area was considered significant according to the Kruskal-Wallis test (chi-squared = 29.482, df = 1, p-value < 0.05) (Figure 4). This significant rise in LST aligns with the global surface temperature increase of 1.1°C above the years 1850-1900 during 2011-2020, with more significant increases over land averaging between 1.34°C and 1.83°C, as reported by the Intergovernmental Panel on Climate Change (IPCC) (IPCC, 2023).

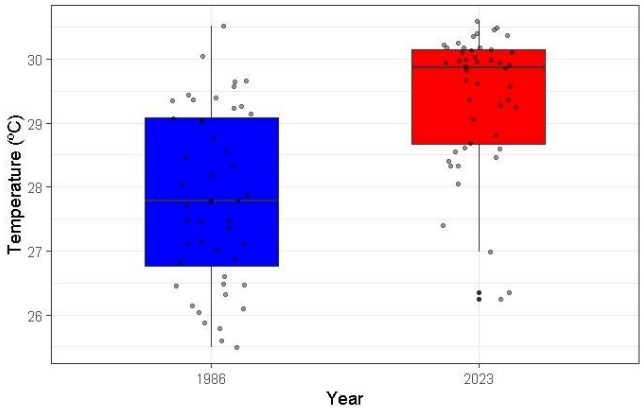

Figure 4. Boxplot of the temperature average in the years 1986 and 2023 for the study area. Each black dot represents the mean for each neighbourhood.

The average increase in LST is in agreement with those found by Furtado et al. (2024), who analyzed the average increases in maximum and minimum temperatures in the period corresponding to the differences between 1985-2002 and 2004-2021, whereby the minimum temperature increased by 0.39 and 0.45ºC in the rainy season, and in the dry season it was 0.53 and 0.60ºC for natural and artificial areas. Also, according to the authors, the maximum temperature increased by 0.58 and 0.62ºC for natural and artificial areas in the rainy season, while in the dry season, it was 0.83ºC and 0.97ºC for natural and artificial areas, respectively. Dias et al. (2021) also found significant increases in minimum, maximum, and compensated temperatures in Belém and Manaus on a scale of 1 to 1.5 ºC from 1999-2008 and 2009-2018.

Another factor that may explain the increase in temperature besides urban expansion and vegetation suppression over the years in the metropolitan area of Belém, as reported by Furtado et al. (2024) and Dias et al. (2021), is the influence of the El Niño-Southern Oscillation (ENSO), since in the period of 1986 (considering the 3-month moving average of sea surface temperature anomalies referring to July) it was considered a period of neutrality, on the other hand in 2023 in the same period in July there was a strong influence of El Niño (NOAA, 2024).

4.3 Urban Heat Island Changes

The UHI for 1986 and 2023 (Figure 5) shows an expansion, particularly of the Extremely Strong UHI classes towards the north, similar to the pattern observed with the LST. This result highlights that most of the urban area of Belém has UHI regions throughout the neighbourhoods within the study area.

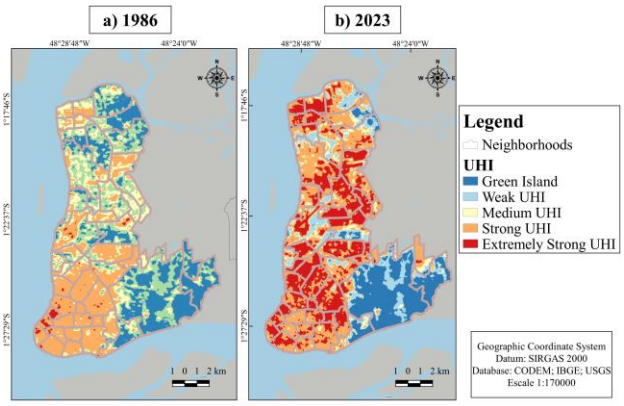

Figure 5. UHI of the years 1986 and 2023 for the urban area of the Belém.

This expansion of the UHI was quantified (Table 4). In 1986, the most representative classes were Strong UHI and Weak UHI, accounting for 30.77% and 25.97%, respectively, while the Extremely Strong UHI class was the smallest, at only 0.93%. By 2023, there was a significant increase in the Extremely Strong UHI and Strong UHI classes, representing 62.53% of the entire urban area. Notably, the Extremely Strong UHI class saw an increase of 2,942.68%.

Classes	1986		2023	
	Area (km²)	Area (%)	Area (km²)	Area (%)
Green Island	41.64	23.50	30.15	17.01
Weak UHI	46.02	25.97	22.65	12.78
Medium UHI	33.39	18.84	13.60	7.67
Strong UHI	54.52	30.77	60.91	34.37
Extremely Strong UHI	1.64	0.93	49.90	28.16

Table 4. Area and percentages of UHI in 1986 and 2023.

Other classes, such as Green Island, Weak UHI, and Medium UHI, showed a decrease of 27.59%, 50.78%, and 59.27% in their total area, respectively. This decrease is associated with reducing green areas and suppressing vegetation in the city, as discussed in previously mentioned research.

4.4 Moran Index Analysis

The results showed that in 1986, the peaks of maximum temperature of neighbourhoods were assigned in the Reduto (32.43°C), São Bráz (31,76°C), and Jurunas (31,76°C). The peaks of the minimum temperature of neighbourhoods were found in Aura (22,80°C), Águas Negras (23,31°C), and Curió-Utinga (23,33°C). The UHI neighbourhood’sneighborhood's results concerning maximum and minimum were the same as LST, with values ranging between -1°C (Green Island) and 5,60°C (Extremely Strong UHI).

In 2023, the results showed the peaks of maximum temperature were found in Tenoné (36,88°C), Sacramenta (35,59°C), and Parque Guajará (34,66°C). The minimum peaks are in Maracacuera (25,17°C), Curió-Utinga (25,35°C), and Universitário (25,40°C). These LST results were the same neighbourhoods found by UHI as Green islands, in other words, below -1°C and above 6,00°C (Extremely Strong UHI).

According to other local studies, the Global Moran's I Index (Figures 6 and 7) presented a value of 0,642, which is considered good (Silva et al., 2021). Regarding the Local Moran Index, the neighbourhoods that present the most correlation high-high were Campina, Cidade Velha, Cremação, Condor, Fátima, Jurunas, Nazaré, Pedreira, Reduto, São Braz e Umarizal. On the other hand, the neighbourhoods that presented the most correlation Low-Low were Águas Lindas, Aurá, Curió-Utinga, Guanabara, and Parque Guajará.

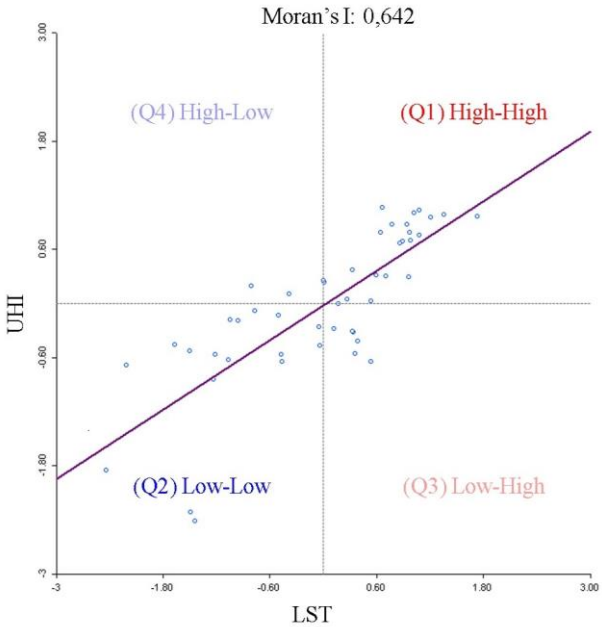

Figure 6. Scatterplot of Moran's I index.

The spatial correlation in these neighbourhoods is associated with the high and low average values between LST and UHI that remained in the respective years. This indicates a degree of spatial variation in magnitude between the variables, consequently presenting this trend with their neighbours. This trend with the neighbourhood is associated with the characteristics of urbanization and afforestation (Figure 7), in which the areas that presented high-high correlation have greater anthropization and urban verticalization.

Silva Júnior et al. (2012) and Lola et al. (2013) also found high values of Heat Index (HI) and air temperature in the central neighborhoods of Belém, falling within the Caution and Extreme Caution ranges regarding thermal comfort. However, the Curió-Utinga neighbourhood presented lower values, indicating complete thermal comfort, which was also observed in this research (Silva Júnior et al., 2012).

The maximum peak temperature values found in the year 2023 in the neighbourhoods of Tenoné, Sacramenta, Parque Guajará, Mangueirão, Castanheira, Tapanã, Val de Cans, Bengui, Pratinha, Parque Verde, Reduto, Batista Campos, Campina de Icoaraci, Maracacuera, and Coqueiro were above 32ºC, considered at HI alert levels as extreme caution and a state of medical emergency in the studies developed by Silva Júnior et al. (2012) and Espinoza et al. (2023) in the cities of Belém and Manaus respectively.

In the general average of the hottest neighborhoods, Reduto (30.51ºC), Campina (30.05ºC), and Umarizal (29.65ºC) stood out as the hottest in 1986. In 2023, the hottest neighbourhoods

were Reduto again (30.59ºC), Fátima (30.48ºC), and Sacramenta (30.46ºC). These average temperatures are classified as severe thermal stress and caution (Espinoza et al., 2023; Silva Júnior et al., 2012). In contrast, the neighbourhoods with the best thermal comfort on average in 1986 were Aurá (25.49ºC), Águas Lindas (25.59ºC), and Águas Negras (25.79ºC). In 2023, the neighbourhoods with the lowest average temperatures were Aurá (26.25ºC), Curió-Utinga (26.36ºC), and Universitário (26.98ºC). Notably, the temperature differences between the hottest and coldest neighbourhoods (Reduto and Aurá) were 5.02ºC in 1986 and 4.34ºC in 2023. This result aligns with previous research findings, indicating that areas farther from the city centre have better thermal comfort than those closer to the city centre, which have greater soil impermeability and less afforestation.

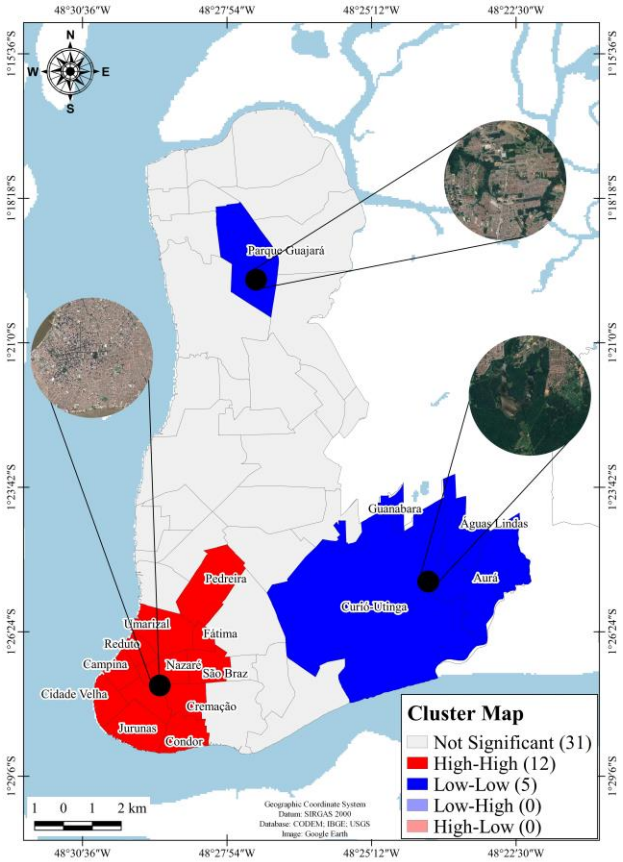

Figure 7. Cluster Map for LST and UHI.

Therefore, the local Moran's I Index results (Figure 7) reflect that where there are high LST and UHI, these are induced by urbanization and low arborization, mainly in the centre areas. This problem can impact people's health due to a temperature increase. The insights of this research can help to understand climate change in Belém and better support the management of the city by decision-makers and urban planners, focusing on neighbourhoods that present high-value temperatures.

5. Conclusions

The assessment of UHI in the urban area of Belém in the years 1986 and 2023 showed that there was an expansion mainly from the south to the north due to the average increase in LST on the scale of 1.5ºC on average, with an annual increase of 0.04ºC over the 37 years of analysis. This increase was significant according to the Kruskal-Wallis test, being explained by the advance of urbanization, urban verticalization, and the influence of El Niño given the reduction of natural areas in Belém, as reported by other research. The urban area of Belém presented a spatial autocorrelation of magnitude due to the correlation of LST and UHI; on the other hand, the areas further away from the centre, especially the Aurá neighbourhood, presented the most thermally comfortable. The neighbourhood most considered the hottest on average was Reduto, with temperatures averaging 30ºC. Therefore, these insights can help decision-makers and urban planners as a way to focus on the hottest neighbourhoods and promote measures that reduce the increase in temperature and projects focused on civil construction, nature-based solutions, and urban afforestation.

References

Almeida, C. R. D., Teodoro, A. C., Gonçalves, A., 2021: Study of the urban heat island (UHI) using remote sensing data/techniques: A systematic review. *Environments*, *8*(10), 105. https://doi.org/10.3390/environments8100105.

Alvares, C. A., Stape, J. L., Sentelhas, P. C., Gonçalves, J. D. M., & Sparovek, G., 2013: Köppen’s climate classification map for Brazil. *Meteorologische zeitschrift*, *22*(6), 711-728.

Aslan, N., & Koc-San, D., 2023. The Effects of Land Cover Changes on Land Surface Temperatures. *The International Archives of the Photogrammetry, Remote Sensing and Spatial Information Sciences*, *48*, 1311-1318. https://doi.org/10.5194/isprs-archives-XLVIII-1-W2-2023-1311-2023.

Batoni, A. G., do Valle Junior, R. F., de Melo, M. M. A. P., de Morais Fernandes, G. H., Feitosa, T. H. S., Fernandes, L. F. S., ... & Pacheco, F. A. L., 2024: Remote sensing of hazards: The spatio-temporal evolution of land surface temperature over tailings flows and related drivers. *Remote Sensing Applications: Society and Environment*, *35*, 101237. https://doi.org/10.1016/j.rsase.2024.101237.

Câmara, G., Carvalho, M. S., Cruz, O. G., Correa, V., 2004. Análise Espacial de Áreas. in *Análise Espacial de Dados Geográficos*. Vol. 1, edited by S. Druck, M. S. Carvalho, G. Câmara, and A. M. V. Monteiro. Brasilia: EMBRAPA.

Carrasco, R. A., Pinheiro, M. M. F., Junior, J. M., Cicerelli, R. E., Silva, P. A., Osco, L. P., & Ramos, A. P. M., 2020: Land use/land cover change dynamics and their effects on land surface temperature in the western region of the state of São Paulo, Brazil. *Regional Environmental Change*, *20*, 1-12. https://doi.org/10.1007/s10113-020-01664-z.

Dias, T. S. S., Souza, E. B., Franco, V. S., Almeida, Á. J., Pinto, M. C. T., Mendoza, R. R., ... & Silva, M. V. S., 2021: Urban Environment and the Air Temperature Trend: The Case of the Metropolis of Brazilian Amazon. *Revista Brasileira de Geografia Física*, *14*(01), 159-171.

Diem, P. K., Nguyen, C. T., Diem, N. K., Diep, N. T. H., Thao, P. T. B., Hong, T. G., & Phan, T. N., 2024: Remote sensing for urban heat island research: Progress, current issues, and perspectives. *Remote Sensing Applications: Society and Environment*, *33*, 101081. https://doi.org/10.1016/j.rsase.2023.101081.

Espinoza, N. S., Santos, C. A. C., Oliveira, M. B. L., Silva, M. T., Santos, C. A. G., Silva, R. M., ... & Ferreira, R. R., 2023: Assessment of urban heat islands and thermal discomfort in the Amazonia biome in Brazil: A case study of Manaus city. *Building and Environment*, *227*, 109772. https://doi.org/10.1016/j.buildenv.2022.109772.

Faisal, A. A. K., Al Rakib, A., Akter, K. S., Jahir, D. M. A., Sikdar, M. S., Ashrafi, T. J., ... & Rahman, M. M., 2021: Assessing and predicting land use/land cover, land surface temperature and urban thermal field variance index using Landsat imagery for Dhaka Metropolitan area. *Environmental Challenges*, *4*, 100192. https://doi.org/10.1016/j.envc.2021.100192.

Furtado, L. S., Pereira, R. V. S., & de Souza, E. B., 2024: Hemeroby Mapping of the Belém Landscape in Eastern Amazon and Impact Study of Urbanization on the Local Climate. *Urban Science*, *8*(1), 15. https://doi.org/10.3390/urbansci8010015.

Ghasempour, F., Sekertekin, A., & Kutoglu, S. H., 2023. How landsat 9 IS superior to landsat 8: Comparative assessment of land use land cover classification and land surface temperature. *ISPRS Annals of the Photogrammetry, Remote Sensing and Spatial Information Sciences*, *10*, 221-227. https://doi.org/10.5194/isprs-annals-X-4-W1-2022-221-2023.

IBGE. Instituto Brasileiro de Geografia e Estatística., 2010. Censo Demográfico. Rio de Janeiro: IBGE. Retrieved from: http://www.censo2010.ibge.gov.br (Accessed on 1 February 2021).

IBGE. Instituto Brasileiro de Geografia e Estatística., 2022. Panorama das Cidades Brasileira; IBGE: Rio de Janeiro, Brazil. Retrieved from: https://cidades.ibge.gov.br (Accessed on 20 February 2023).

IPCC – Intergovernmental Panel on Climate Change, 2023. Sections. In: Climate Change 2023: Synthesis Report. Contribution of Working Groups I, II and III to the Sixth Assessment Report of the Intergovernmental Panel on Climate Change [Core Writing Team, H. Lee and J. Romero (eds.)]. IPCC, Geneva, Switzerland, pp. 35-115, doi: 10.59327/IPCC/AR6-9789291691647 (Accessed on 15 July 2024).

Kafy, A. A., Al Rakib, A., Fattah, M. A., Rahaman, Z. A., & Sattar, G. S., 2022. Impact of vegetation cover loss on surface temperature and carbon emission in a fastest-growing city, Cumilla, Bangladesh. *Building and Environment*, *208*, 108573. https://doi.org/10.1016/j.buildenv.2021.108573.

Lola, A. C., Silva, J., Cunha, A. C., Galbraith, D. G., & Feitosa, J. R. P., 2013: Distribuição geoespacial e horária da temperatura do ar na cidade de Belém–PA: Estudo de caso em 1995. *Brazilian Geographical Journal: Geosciences and Humanities research medium*, *4*(1), 3.

Moreira, F. D. S. D. A., & Vitorino, M. I., 2017: Relação de áreas verdes e temperatura da superfície para a cidade de Belém. *Papers do NAEA*, *369*, 1-25.

NOAA. Nacional Oceanic and Atmospheric Administration., 2024. El Niño/Southern Oscillation (ENSO). Cold & Warm Episodes by Season. Maryland: NOAA. Retrieved from: https://origin.cpc.ncep.noaa.gov/products/analysis_monitoring/ensostuff/ONI_v5.php (Accessed on 10 July 2024).

Rahaman, Z., Kafy, A., Saha, M., Rahim, A., Almulhim, A., Rahaman, S., Fattah, M., Rahman, M., Kalaivani, S., Faisal, A., Rakib, A., 2022: Assessing the impacts of vegetation cover loss on surface temperature, urban heat island and carbon emission in Penang city, Malaysia. *Building and Environment*, 222, 109335. https://doi.org/10.1016/j.buildenv.2022.109335.

Rizwan, A. M., Dennis, L. Y., & Chunho, L. I. U., 2008: A review on the generation, determination and mitigation of Urban Heat Island. *Journal of environmental sciences*, *20*(1), 120-128. https://doi.org/10.1016/S1001-0742(08)60019-4.

Silva Junior, J. D. A., Costa, A. C. L., Pezzuti, J. C. B., Costa, R. F., & Galbraith, D., 2012: Análise da distribuição espacial do conforto térmico da cidade de Belém, PA no período menos chuvoso. *Revista Brasileira de Geografia Física*, *5*(2), 218-232.

Silva, M. T., Margalho, E. D. S., Serrão, E. A. D. O., Souza, A. C. D., Soares, C. D. S., Santos, C. A. C. D., & Silva, B. B. D., 2021: Application of Spatial Modeling of Biophysical Variables in an Urbanized Area in the Amazon: The Case of the Metropolitan Area of Belém-Pará. *Revista Brasileira de Meteorologia*, *36*, 271-283. https://doi.org/10.1590/0102-77863620063.

Silva, R. M., Lopes, A. G., Santos, C. A. G., 2023: Deforestation and fires in the Brazilian Amazon from 2001 to 2020: Impacts on rainfall variability and land surface temperature. *Journal of Environmental Management*, *326*, 116664. https://doi.org/10.1016/j.jenvman.2022.116664.

Velastegui-Montoya, A., Montalván-Burbano, N., Carrión-Mero, P., Rivera-Torres, H., Sadeck, L., & Adami, M., 2023: Google Earth Engine: a global analysis and future trends. *Remote Sensing*, *15*(14), 3675. https://doi.org/10.3390/rs15143675.

Xu, L. Y., Xie, X. D., & Li, S., 2013: Correlation analysis of the urban heat island effect and the spatial and temporal distribution of atmospheric particulates using TM images in Beijing. *Environmental Pollution*, *178*, 102-114. https://doi.org/10.1016/j.envpol.2013.03.006.

Zhou, D., Zhao, S., Zhang, L., Sun, G., & Liu, Y., 2015: The footprint of urban heat island effect in China. *Scientific Report*, 5, 11160. https://doi.org/10.1038/srep11160.

Waleed, M., Sajjad, M., Acheampong, A. O., & Alam, M. T., 2023: Towards sustainable and livable cities: leveraging remote sensing, machine learning, and geo-information modelling to explore and predict thermal field variance in response to urban growth. *Sustainability*, *15*(2), 1416. https://doi.org/10.3390/su15021416.

Waleed, M., Sajjad, M., 2022: Leveraging cloud-based computing and spatial modeling approaches for land surface temperature disparities in response to land cover change: evidence from Pakistan. *Remote Sensing Applications: Society and Environment*, *25*, 100665. https://doi.org/10.1016/j.rsase.2021.100665.

Wang, M., Zhang, Z., Hu, T., Wang, G., He, G., Zhang, Z., Liu, X., 2020: An efficient framework for producing Landsat-based land surface temperature data using Google Earth engine. *IEEE Journal of selected Topics in applied earth observations and remote sensing*, *13*, 4689-4701. https://doi.org/10.1109/JSTARS.2020.3014586.